Iraqi Journal of Physics, 2024
https://doi.org/10.30723/ijp.v22i3.1265
Vol. 22, No. 3, PP. 67-77
P-ISSN: 2070-4003
E-ISSN: 2664-5548

Synthesis of PPy-MnO_2 Nanocomposite for Utilization in Supercapacitor Applications

Firas J. Hameed[1a*] and Isam M. Ibrahim[1b]
[1] *Department of Physics, College of Science, University of Baghdad, Baghdad, Iraq*
[b]E-mail: drissamiq@gmail.com
[a*]Corresponding author: firasalhbolee@gmail.com
Dr. Isam M. Ibrahim is a journal editor, but he did not participate in the peer review process other than as an author. The authors declare no other conflict of interest.

Abstract

Polypyrrole (PPy) nanocomposites were prepared using chemical oxidation and were combined with manganese oxide (MnO_2) nanoparticles. The PPY-MnO_2 nanocomposite was synthesized by integrating PPy nanofibers with varying volume ratio percentages of MnO_2 dopant (10, 30, and 50% vol. ratio). The structural features of the PPy and PPy-MnO_2 nanocomposite were investigated using X-ray diffraction (XRD). Fourier transfor infrared (FTIR) spectroscopy was used to demonstrate the molecular structures of primary materials and the final product of PPy, MnO_2, and PPy- MnO_2 nanocomposites. Field Emission Scanning Electron Microscopy (FESEM) showed that the morphology of PPy consisted of a network of nanofibers. Increasing the volume ratios of manganese oxide added to the PPY nanofiber led to the increase of manganese oxide nanoparticles on the surface of the PPY nanofiber network. This resulted in a noticeable alteration in the structure of the nanocomposite. It has been observed that the nanocomposites demonstrate a significant level of pseudocapacitive activity. The highest capacitance of 236 F/g was observed when pure PPy was doped with 30% MnO_2 compared to 125 F/g of the pure PPy.

Article Info.

Keywords:
Polypyrrole (PPy), Manganese oxide (MnO_2), Structural Properties, Supercapacitor, Capacitance.

Article history:
Received: Apr.18, 2024
Revised: Jun. 30, 2024
Accepted: Jul. 14, 2024
Published: Sep.01, 2024

1. Introduction

Pseudocapacitance supercapacitors are environmentally friendly power sources commonly utilized in many applications, such as portable electronics, digital communication systems, power backup systems, and hybrid electric cars [1-4]. The performance of supercapacitors, including specific capacitance, rate capability, and cycling stability, is greatly influenced by the properties of electrode materials. Therefore, there have been many efforts in recent years to create effective electrode materials [5]. Manganese oxide (MnO_2) widely used in energy storage devices (e.g., lithium-ion batteries, capacitors), catalysts, adsorbents, sensors and imaging, therapeutic activity, is a significant pseudocapacitance material known for its high theoretical capacitance of 1370 F/g [6], affordability, eco-friendliness, and availability in nature. Yet, its use in supercapacitors may be restricted by its inadequate electrical conductivity [6]. Polypyrrole (PPy) is a conductive polymer with high electrical conductivity, unique doping/dedoping properties, environmental durability, excellent biocompatibility, and versatile production methods [7-9]. Conductive polymers are characterized by the conjugated double bonds along the polymer chain [10]. The polymer's composition and the positioning of nanoparticles within the polymer matrix have been found to impact several characteristics [11]. PPy is used in various applications, including manufacturing batteries, sensors, electrical devices, and supercapacitors [12]. Adding

MnO_2 can significantly enhance the electrical conductivity of PPy. The PPy-MnO_2 composites have gained attention in research due to the synergistic effect of MnO_2 and PPy. The PPy-MnO_2 composites exhibit outstanding pseudocapacitive performance in a neutral electrolyte, making them appealing electrode materials for supercapacitors [13-15]. PPy and other conducting polymers have significant charge storage capacities, but their mechanical and long-term stability are not good enough. Supercapacitor electrodes, a novel mixture of metal oxide particles spread across a sizable surface area supported by conducting polymer, seem promising [16]. PPy offers a very large surface area for dispersing MnO_2, allowing it to develop into nanoscale particles with a high active surface area for redox reactions. The MnO_2 particles offer firm support and an interconnected electrical pathway to PPy by connecting the polymer chains, enhancing charge exchange efficiency and stability during redox cycling.

This work presents the synthesis, electrochemical behaviour, and structural properties of the PPy-MnO_2 nanocomposite electrodes designed for supercapacitors [17].

2. Experimental Part

2.1. Preparation of PPy Nanofiber

The polypyrrole nanofibers were constructed using the approach outlined by Yang and Li [18]. 0.818 g of methyl orange was uniformly distributed in 60 ml of distilled water. 2.237 g of ferric chloride was mixed with the methyl orange liquid solution with agitation at a speed of 80 rpm and placed in an ice bath with 1ml of pyrrole. The mixture was stirred continuously for 1 day till it turned black. The precipitate was subjected to several washes with ethanol and distilled water, followed by filtration and drying for 60 minutes. All the chemicals used in this work were purchased from Alfa Aesar (Germany).

2.2. Preparation of Polypyrrole-Manganese oxide (PPy-MnO_2) Nanocomposite

A homogenous dispersion was created by dissolving MnO_2 in distilled water, combining it with PPy at volume ratios of 10, 30, and 50%, and subjecting it to ultrasonic vibrations for one hour.

2.3. Electrode Preparation

To prepare the PPy-MnO_2 electrode, the PPy-MnO_2 nanocomposite of 10, 30, and 50% MnO_2 ratios was deposited on a 1x1 cm^2 nickel foam substrate via drop casting. The PPy-MnO_2/nickel foam sample underwent testing by cyclic voltammetry (CV), galvanostatic charge-discharge analysis (GCD), and electrochemical impedance spectroscopy (EIS) in a 1 mil volume of concentrated sulfuric acid solution with a 100% concentration. The electrode made of PPy- MnO_2 had a mass of 0.1 mg.

3. Results and Discussion

3.1. X-ray Diffraction

Fig. 1 illustrates the X-ray diffraction (XRD) patterns of PPy nanofiber, and PPy-MnO_2 nanocomposite. The XRD pattern PPy has a diffraction peak at $2\theta = 20.35°$; it displays a broad peak for 2θ values ranging from 13^o to 29^o. This peak is characterized by weak intensity and broadness, indicating that the PPy is amorphous [19]. It is well known that MnO_2 has strong diffraction peaks suggesting that the material is crystalline in its natural state. XRD patterns of PPy-MnO_2 nanocomposite of 10, 30, and 50% MnO_2 show diffraction peaks at 33.3^o, 38.5^o, 46.5^o, 49.7^o, 56^o, and 66.2^o correlated to

the distinctive peaks of MnO_2 corresponding to the crystal planes of (111), (200), (202), (311), (222), and (400), respectively, in accordance with code (Crystallography Open Database) 9008674 and 1010436. These results agree with those reported by Wyckoff [20] and Ruhemann [21]. The XRD patterns of PPy-MnO_2 nanocomposites make it abundantly evident that the nanocomposites exhibit just six peaks of MnO_2, whereas the broad peak from PPy is observed with a significantly lower intensity. During the polymerization reaction, the crystal structure of the MnO_2 particles could be distorted into an amorphous phase, which is indicated by the six peaks [22].

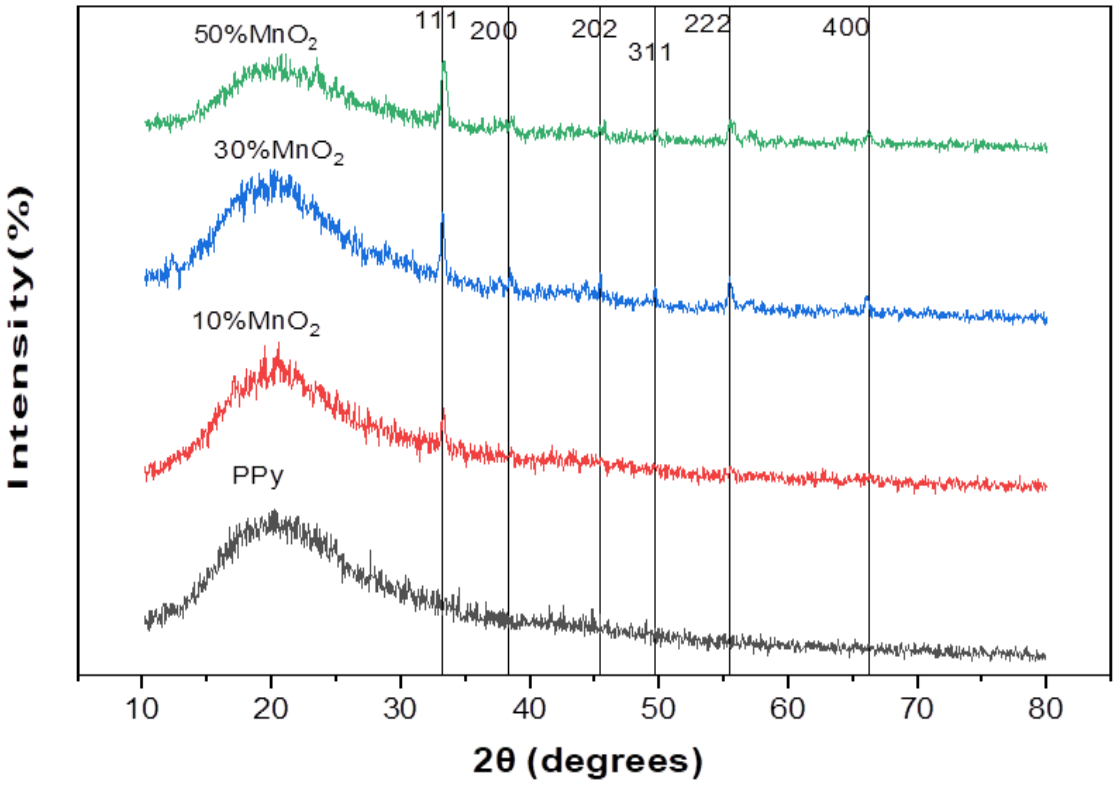

Figure 1: XRD patterns of PPy and PPy-MnO_2 nanocomposite of different MnO_2 percentages.

3.2. Fourier Transform Infrared Analyses (FTIR)

Active synthesis of the polypyrrole-Manganese oxide composite was verified using FTIR spectra analysis. Fig. 2 shows the spectra of PPy, and PPy-MnO_2 nanocomposite with varying percentages of MnO_2 (10, 30, and 50%). The signal detected at 1050 cm^{-1} and 1043 cm^{-1} is associated with O-H bending vibration of PPy and PPy-MnO_2, respectively [23]. Mn-O vibration is the cause of the signal observed at 559 cm^{-1} and 449 cm^{-1} [14]. The peak at 1590 cm^{-1} is associated with the stretching vibration of the -OH group, whereas the peak at 1080 cm^{-1} corresponds to N-H in-plane deformation vibration of the pyrrole ring [14, 24]. The peaks in the PPy FTIR spectrum at 3140 cm^{-1} and 831 cm^{-1} correspond to the C-H stretching vibration mode [25]. The peak at 1080 cm^{-1} in the PPy spectrum changed to 1089 cm^{-1} in the PPy-MnO_2 nanocomposite due to an interaction between PPy and MnO_2 affecting the N-H in-plane deformation vibration of the pyrrole ring. The peak at 3730 cm^{-1} corresponds to the polypyrrole rings N-H. The peaks at 449 cm^{-1}, 1050 cm^{-1}, 1590 cm^{-1}, and 831 cm^{-1} in the PPy spectrum have shifted to 471 cm^{-1}, 1600 cm^{-1}, and 871 cm^{-1} in the PPy-MnO_2 nanocomposite spectrum, respectively, due to the interaction between PPy and MnO_2

affecting the Mn-O vibration, O-H bending vibration, stretching vibration of the -OH group and C-H stretching vibration, respectively [14, 23-25].

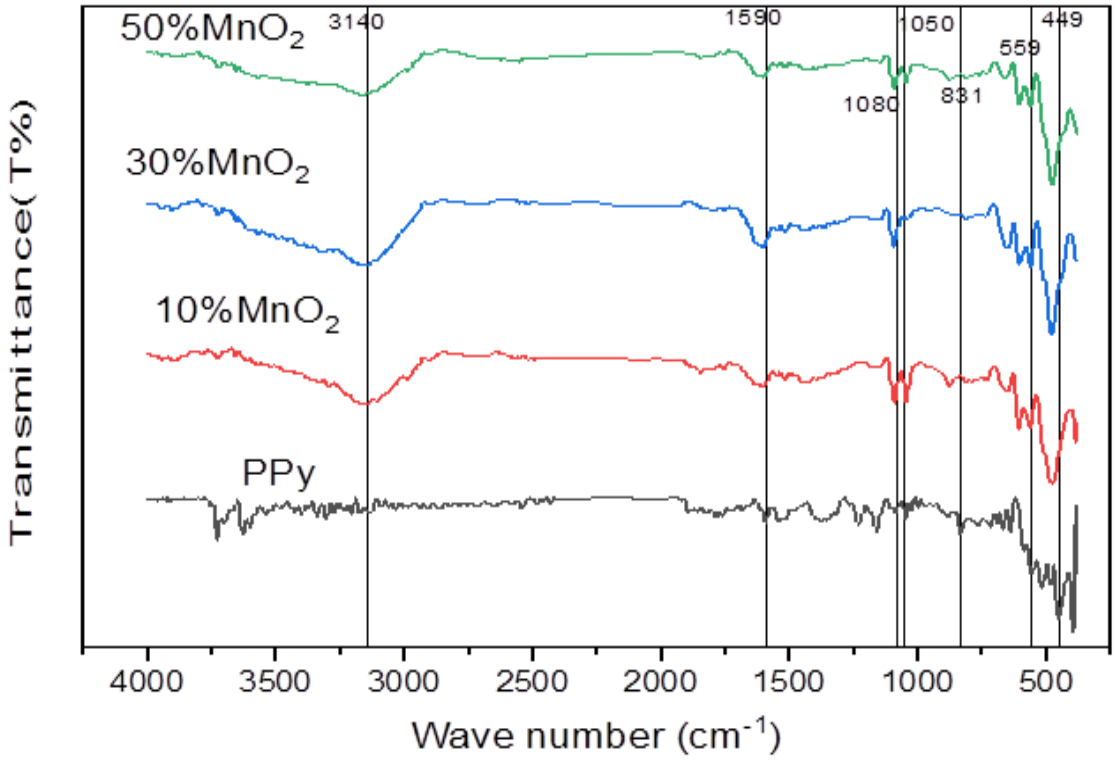

Figure 2: FTIR spectra of PPy and PPy-MnO_2 nanocomposite of different MnO_2 percentages.

3.3. Analysis of the Field Emission Scanning Electron Microscopy (FE-SEM)

The surface morphology of as-made PPy and PPy-MnO_2 nanocomposite of different MnO_2 percentages was analyzed using the field emission scanning electron microscopy (FE-SEM), as depicted in the microstructure images shown in Figs. 3a and 3b at magnifications of x 350000 and x 135000, respectively. PPy was chemically synthesized using the method of chemical oxidation and an ice bath, as previously mentioned. It is observed from the images of the PPy that the substance consisted of nanofibers. The morphology of the PPy-MnO_2 nanocomposites exhibited a uniformity in the arrangement of PPy nanofibers and the MnO_2 nanoparticles. The scaffold made of PPy consisted of interconnected fibers/particles, adding manganese oxide nanoparticles results in the formation of a three-dimensional compound thus conduction will be three-dimensional, i.e., it will be conductive from all directions.

The bulk of these nanofibers have diameters ranging from 50 to 100 nm. The PPy-MnO_2 nanocomposite exhibited the formation and aggregation of PPy fibers on the surface due to the interactions between the fibers and MnO_2 particles, as observed in the FESEM images. With the addition of MnO_2, an attraction occurs between the PPy and the MnO_2, which increases as the percentage of the added MnO_2 increase leading to small blocks forming on the surface of the PPy. The obtained images are almost identical to those presented by Khan et al. [24] and Bahloul et al. [26].

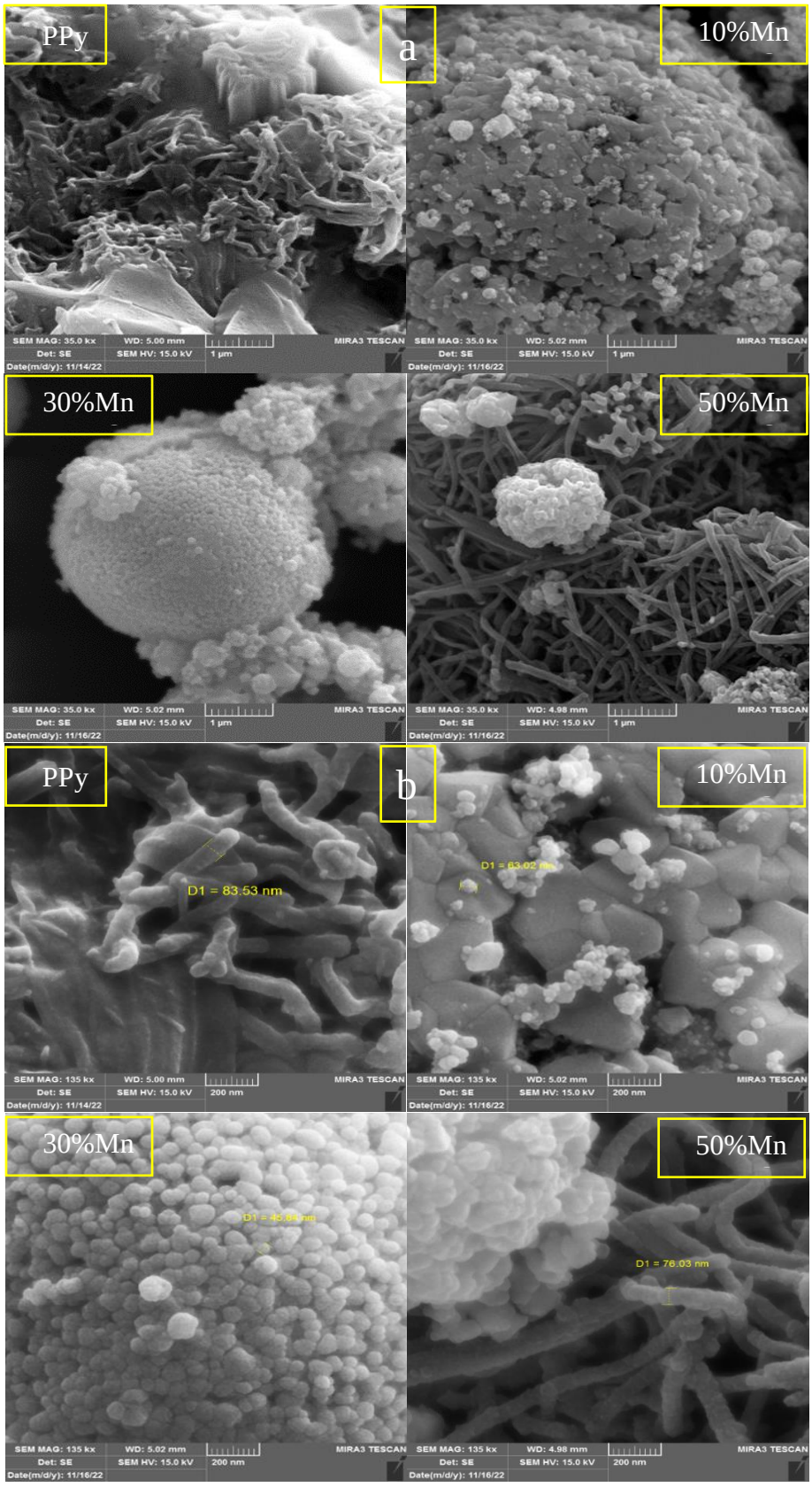

Figure 3: Field Emission Scanning Electron Microscope (FESEM) images of PPy, (a) PPy-10%MnO_2, PPy-30%MnO_2, and PPy-50%MnO_2, (b) PPy-10%MnO_2, PPy-30%MnO_2, and PPy-50%MnO_2. (x 135000 magnification).

3.4. Supercapacitor's figure of merit

The electrochemical measurement of the supercapacitor was initially assessed through a systematic measurement using Cyclic Voltammetry (CV), Galvanostatic Charge/Dscharge (GCD), and Electrochemical Impedance Spectroscopy (EIS) in a conventional three-electrode setup [27, 28].

3.4.1. Cyclic Voltammetry (CV)

Cyclic voltammetry (CV) is a powerful electrochemical technique that may be used to determine the predominant electron transfer pathway as a function of time and applied potential [29]. Fig. 4 (a-c) displays the outcomes of the cyclic voltammetry analysis conducted on PPy and PPy-MnO_2 nanocomposites. The anode peaks are observed at (3.49, 4.2, 5.2, 3.25), (5.88, 10.1, 10.3, 7.65), and (12.4, 17.7, 15.2, 12.1) mA for the pure PPY and 10, 30 and 50% MnO_2 in the PPy-MnO_2 nanocomposites, respectively, with the repetitive application of the scan rates of (50, 100, and 150). The materials exhibited electrochemical activity within a specific range of potential, as indicated by the CV data. CV curves (voltammograms) exhibited a pair of clearly defined redox peaks, a typical characteristic of battery-type electrodes [30]. The electrochemical properties of both PPy and MnO_2 are combined in the PPy-MnO_2 composite film. The PPy-MnO_2 nanocomposite thin film exhibited an electrochemical reaction at potentials below 0.75 V, as depicted in Fig. 4. The anode electrode functioned as the emitter of positive charges, while the cathode electrode served as the store for positive charge carriers within the PPy and PPy-MnO_2. This mechanism operates throughout the discharge procedure. When a cathodic voltaic (CV) reaction occurs, the cathode side of the system becomes black, while the anode side remains white. Unlike PPy, the Gaussian shape seen in Fig. 4 demonstrates that the electrochemical interaction plays a significantly more important role in PPy-MnO_2 nanocomposites. This could be clarified by harnessing the combined impacts of PPy and MnO_2. The presence of two distinct and prominent redox peaks on each curve depicted in Fig. 4(a-c) indicates the occurrence of a pseudo-capacitative feature of the supercapacitor, which is a result of the Faradaic redox reactions. The PPy-MnO_2 nanocomposite thin film was found to possess similar properties as reported by Sharma et al.[17] and Liao et al. [31]. Organic electrolytes with broad voltage ranges are the preferred option for commercial supercapacitors in terms of energy density; aqueous electrolytes are cost-effective and may be easily managed in a laboratory setting without requiring particular conditions [32].

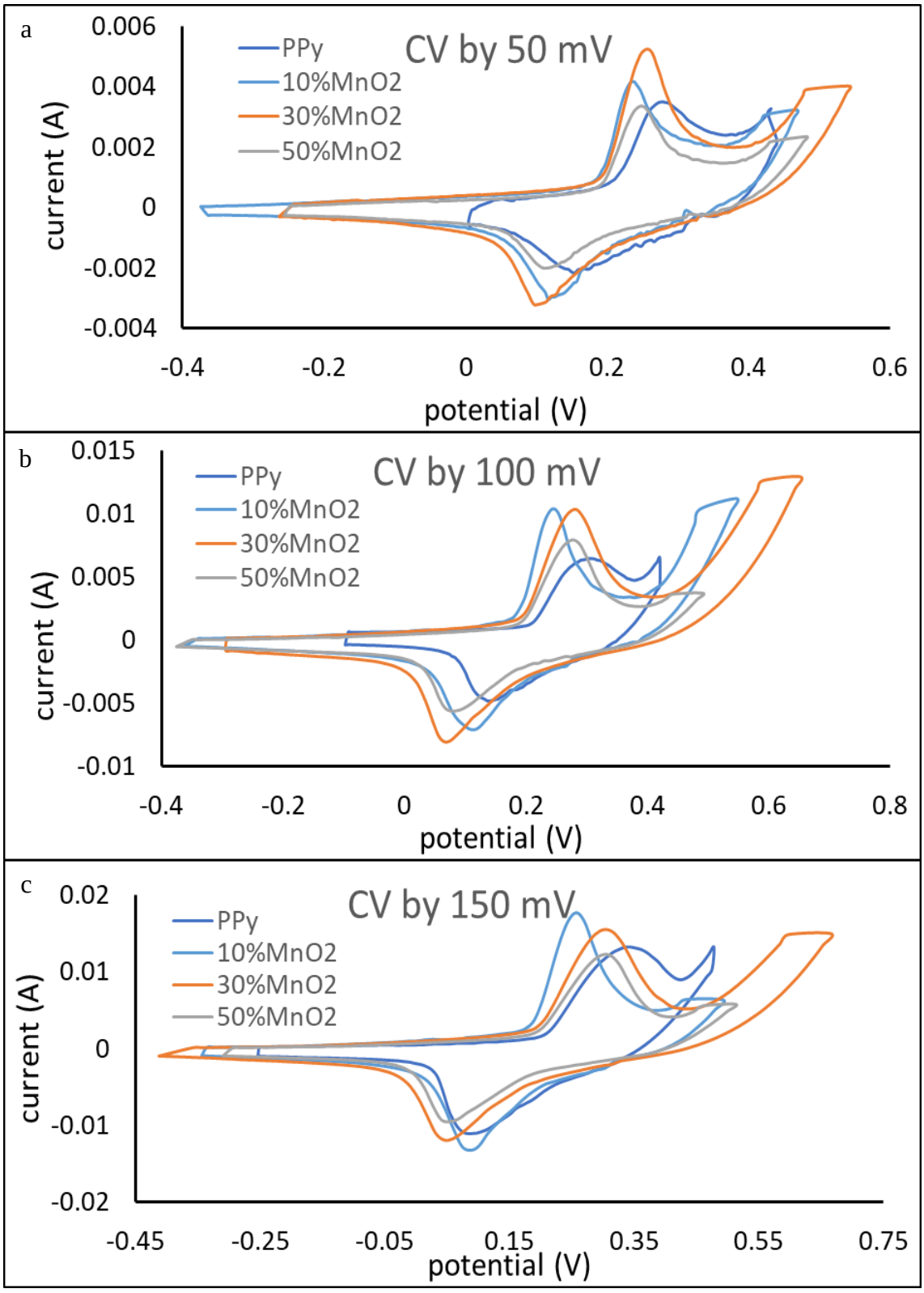

Figure 4: The cyclic voltammograms of PPy and PPy-MnO_2 nanocomposite with different concentrations of MnO_2 at a voltage of (a) 50 mV, (b) 100 mV, (c) 150 mV.

3.4.2. Galvanostatic Charge-Discharge (GCD)

An electrochemical performance assessment of the hybrid PPy-MnO_2 electrode was conducted using a galvanostatic charge/discharge test [33]. To ensure optimal performance of the hybrid system, potential fluctuations for individual electrodes were measured independently when a Ni-foam reference anode was introduced [34]. This was done to determine the most significant working potential range [35]. The potential variations in the negative and positive electrodes were virtually slanting, with one and two stages. These variations occurred when charging and discharging and were similar to the CV data shown in Fig. 4. This is a result of the potential interdependence of redox processes. PPy, a polymer capable of incorporating anions, undergoes p-doping. A polaron is formed when a continuous movement of electrons from a neutral section of their quinoid chains leads to a localized alteration of the positive charge [36]. The PPy and the PPy-MnO_2 electrodes performed effectively within the typical potential ranges throughout the charge/discharge procedures (Fig. 5). In addition, the PPy-MnO_2 hybrid composite electrode had the ability to operate within a working potential window of 0.25 V [35]. The specific capacitance (C), measured in Farads per gram (F/g), can be determined from the CD curve using the following equation [33]:

$$\mathbf{C} = \frac{\boldsymbol{I\Delta t}}{\boldsymbol{\Delta V m}} \qquad \textbf{(1)}$$

where: ΔV represents the potential window in Volts (V) (in this case, it was 0.25 V), I is the discharge current in Amperes (A) (here it was 0.5 mA), Δt is the discharge time in seconds (5s for pure PPy, 7s for PPy:10% MnO_2, 11.8s for PPy:30% MnO_2, and 6.5s for PPy:50% MnO_2), and m is the mass of the PPy or PPy-MnO_2 electrode in grams (in this case it was 0.1 mg). By incorporating 10% MnO_2, the capacity of the PPy was successfully enhanced from 125 (F/g) to 167.46 (F/g); the capacity was further raised to 236 (F/g) for 30% MnO_2. However, when the MnO_2 content was 50%, the capacity declined to 126.45 (F/g). This observed phenomenon can be attributed to the electrostatic attraction between PPy nanofibers and MnO_2, leading to an increase in the surface area and, consequently, the capacitance [37, 38]. In the supercapacitor, the oxidative polymerization procedure in PPy-MnO_2 nanocomposites electrode with a 1 M H_2SO_4 as the electrolyte achieved the greatest capacity value of 236 (F/g).

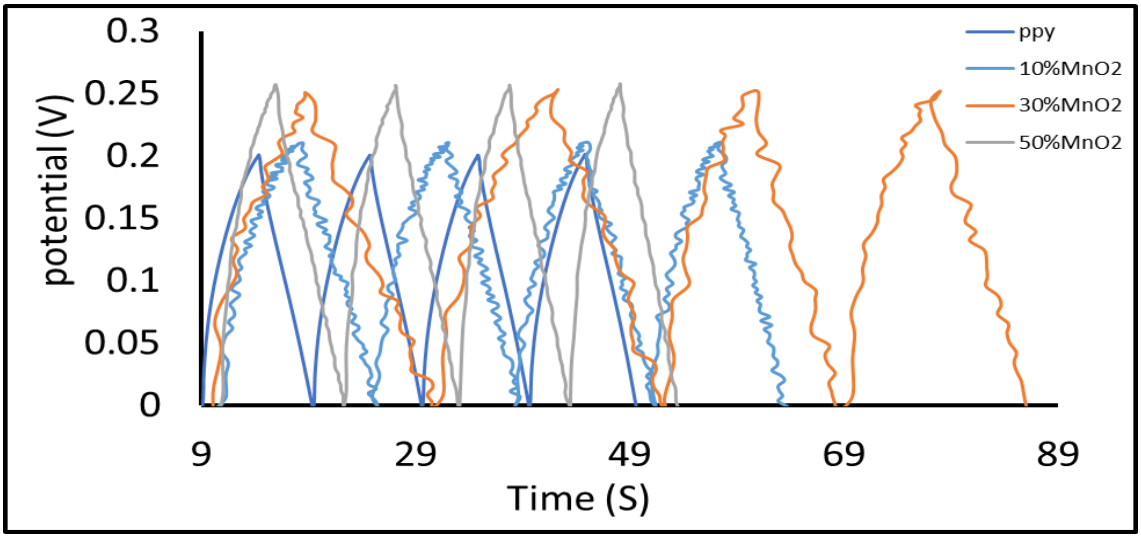

Figure 5: Galvanostatic charge-discharge behavior of pure PPy and PPy-MnO_2 at different MnO_2 percentages.

3.4.3. Electrochemical Impedance Spectroscopy (EIS)

To comprehend the charge transfer of the PPy-MnO_2 electrode material, an electrochemical impedance spectroscopy (EIS) plot was conducted on the PPy samples and PPy-MnO_2 nanocomposites of different MnO_2 percentages (Fig. 6). Nyquist plots, shown in Fig. 6, were evaluated by applying a 5 mV AC voltage of 1 Hz to 1000 kHz frequency range at the open circuit potential. The ohmic resistance can be determined by measuring the real component of the impedance at the high-frequency intercept of the semicircle. At higher frequencies, the narrow semicircle indicates a low transfer resistance of the charge with a slight diffusion at lower frequencies. If the beeline has a 45-° slope in the low-frequency domain, it means that the mechanism was driven by diffusion. Conversely, if the slope was 90°, it means an entirely capacitive behaviour. The Nyquist plot exhibited a semi-circular configuration, signifying a highly proficient transmission of electric charge. This discovery provides more evidence to support the exceptional durability of the PPy-MnO_2 nanocomposite during electrochemical cycling. This material has demonstrated promising potential for use as an electrode in electrochemical supercapacitors [39-42].

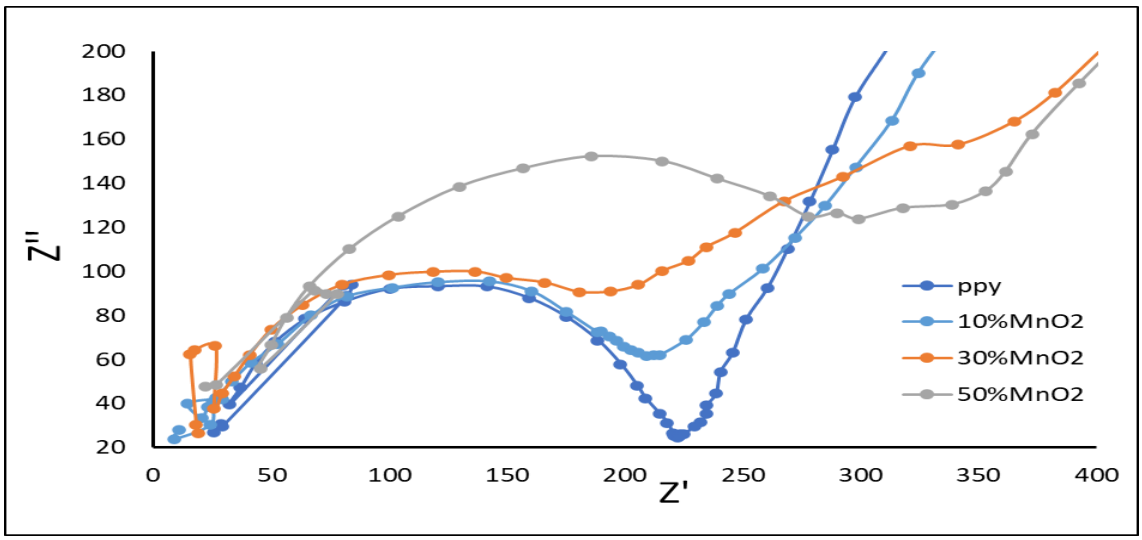

Figure 6: Nyquist curves of the electrochemical impedance spectroscopy of PPy and PPy-MnO_2 of different MnO_2 percentages.

4. Conclusions

PPy nanofiber and PPy-MnO_2 nanocomposite were synthesized using a straightforward technique. The combination of PPy and MnO_2 in a composite film is an excellent material for the electrodes in electrochemical supercapacitors. The GCD curves revealed that pure PPy exhibited much lower capacitance than the PPy combined with MnO_2. PPy nanofibers combined with 30% MnO_2 had the highest capacitance values, reaching 236F/g. Hence, increasing the percentage volume ratio of MnO_2 significantly enhanced the capacitance of supercapacitors.

Conflict of interest

Authors declare that they have no conflict of interest.

References

1. J.-G. Wang, F. Kang, and B. Wei, Prog. Mat. Sci. **74**, 51 (2015). DOI: 10.1016/j.pmatsci.2015.04.003.
2. P.-Y. Tang, L.-J. Han, A. Genç, Y.-M. He, X. Zhang, L. Zhang, J. R. Galán-Mascarós, J. R. Morante, and J. Arbiol, Nano Ener. **22**, 189 (2016). DOI: 10.1016/j.nanoen.2016.02.019.
3. J. S. Lee, D. H. Shin, and J. Jang, Ener. Envir. Sci. **8**, 3030 (2015). DOI: 10.1039/C5EE02076J.
4. Y. Zhao, J. Misch, and C.-A. Wang, J. Mat. Sci. Mat. Elect. **27**, 5533 (2016). DOI: 10.1007/s10854-016-4457-x.
5. J. K. Gan, Y. S. Lim, N. M. Huang, and H. N. Lim, Appl. Surf. Sci. **357**, 479 (2015). DOI: 10.1016/j.apsusc.2015.09.071.
6. F. Shi, L. Li, X.-L. Wang, C.-D. Gu, and J.-P. Tu, RSC Advan. **4**, 41910 (2014). DOI: 10.1039/C4RA06136E.
7. H. Farrokhi, O. Khani, F. Nemati, and M. Jazirehpour, Synth. Metals **215**, 142 (2016). DOI: 10.1016/j.synthmet.2016.02.016.
8. L. Jiang, X. Lu, J. Xu, Y. Chen, G. Wan, and Y. Ding, J. Mat. Sci. Mat. Elect. **26**, 747 (2015). DOI: 10.1007/s10854-014-2459-0.
9. M. A. Salman and S. M. Hassan, Iraqi J. Phys. **19**, 33 (2021). DOI: 10.30723/ijp.19.48.33-43
10. N. J. Abdullah, S. M. Hasan, and A. F. Essa, AIP Conference Proceedings **2372**, 130016 (2021). DOI: 10.1063/5.0065394.
11. H. M. Hawy and I. M. Ali, Optik **262**, 169263 (2022). DOI: 10.1016/j.ijleo.2022.169263.
12. N. J. Abdullah, A. F. Essa, and S. M. Hasan, Iraqi J. Sci. **62**, 138 (2021). DOI: 10.24996/ijs.2021.62.1.13.
13. P. Li, Y. Yang, E. Shi, Q. Shen, Y. Shang, S. Wu, J. Wei, K. Wang, H. Zhu, Q. Yuan, A. Cao, and D. Wu, ACS Appl. Mat. Inter. **6**, 5228 (2014). DOI: 10.1021/am500579c.
14. F. Liang, Z. Liu, and Y. Liu, J. Mat. Sci. Mat. Elect. **28**, 10603 (2017). DOI: 10.1007/s10854-017-6835-4.
15. J. Han, L. Li, P. Fang, and R. Guo, J. Phys. Chem. C **116**, 15900 (2012). DOI: 10.1021/jp303324x.
16. Y. H. Park, K. W. Kim, and W. H. Jo, Polym. Adv. Technol. **13**, 670 (2002). DOI: 10.1002/pat.331.
17. R. K. Sharma, A. C. Rastogi, and S. B. Desu, Electrochim. Acta **53**, 7690 (2008). DOI: 10.1016/j.electacta.2008.04.028.
18. X. Yang and L. Li, Synth. Met. **160**, 1365 (2010). DOI: 10.1016/j.synthmet.2010.04.015.
19. B. T. Raut, M. A. Chougule, A. A. Ghanwat, R. C. Pawar, C. S. Lee, and V. B. Patil, J. Mat. Sci. Mat. Elect. **23**, 2104 (2012). DOI: 10.1007/s10854-012-0708-7.
20. R. W. G. Wyckoff, *Crystal Structures* (New York, Interscience Publishers, 1963).
21. F. Ruhemann, Physik. Ber **16**, 2337 (1935).
22. J. Li, T. Que, and J. Huang, Mat. Res. Bullet. **48**, 747 (2013). DOI: 10.1016/j.materresbull.2012.11.014.
23. Y. Song, M. Shang, J. Li, and Y. Su, Chem. Eng. J. **405**, 127059 (2021). DOI: 10.1016/j.cej.2020.127059.
24. H. Khan, K. Malook, and M. Shah, J. Mat. Sci. Mat. Elect. **29**, 9090 (2018). DOI: 10.1007/s10854-018-8936-0.
25. Y. Chen, X. Zhang, C. Xu, and H. Xu, Electrochim. Acta **309**, 424 (2019). DOI: 10.1016/j.electacta.2019.04.072.
26. A. Bahloul, B. Nessark, E. Briot, H. Groult, A. Mauger, K. Zaghib, and C. M. Julien, J. Pow. Sour. **240**, 267 (2013). DOI: 10.1016/j.jpowsour.2013.04.013.
27. W. Zhao, J. Peng, W. Wang, B. Jin, T. Chen, S. Liu, Q. Zhao, and W. Huang, Nano. Micro. Small **15**, 1901351 (2019). DOI: 10.1002/smll.201901351.
28. Z. Yang, J. Ma, B. Bai, A. Qiu, D. Losic, D. Shi, and M. Chen, Electrochim. Acta **322**, 134769 (2019). DOI: 10.1016/j.electacta.2019.134769.
29. R. Moreno Araújo Pinheiro Lima and H. P. De Oliveira, J. Ener. Stor. **28**, 101284 (2020). DOI: 10.1016/j.est.2020.101284.
30. W. He, G. Zhao, P. Sun, P. Hou, L. Zhu, T. Wang, L. Li, X. Xu, and T. Zhai, Nano Ener. **56**, 207 (2019). DOI: 10.1016/j.nanoen.2018.11.048.
31. X. Liao, C. Pan, Y. Pan, and C. Yin, J. Alloy. Comp. **888**, 161619 (2021). DOI: 10.1016/j.jallcom.2021.161619.
32. N. Sheng, S. Chen, J. Yao, F. Guan, M. Zhang, B. Wang, Z. Wu, P. Ji, and H. Wang, Chem. Eng. J. **368**, 1022 (2019). DOI: 10.1016/j.cej.2019.02.173.
33. A. P. Tiwari, S.-H. Chae, G. P. Ojha, B. Dahal, T. Mukhiya, M. Lee, K. Chhetri, T. Kim, and H.-Y. Kim, J. Coll. Inter. Sci. **553**, 622 (2019). DOI: 10.1016/j.jcis.2019.06.070.

34. K. D. Kumar, T. Ramachandran, Y. A. Kumar, A. a. A. Mohammed, and M. Kang, J. Phys. Chem. Sol. **185**, 111735 (2024). DOI: 10.1016/j.jpcs.2023.111735.
35. B. Dahal, T. Mukhiya, G. P. Ojha, A. Muthurasu, S.-H. Chae, T. Kim, D. Kang, and H. Y. Kim, Electrochim. Acta **301**, 209 (2019). DOI: 10.1016/j.electacta.2019.01.171.
36. S. Ghosh, *Conjugated Polymer Nanostructures for Energy Conversion and Storage Applications* (Kolkata, India, John Wiley & Sons, 2021).
37. W. Xu, L. Zhang, K. Zhao, X. Sun, and Q. Wu, Electrochim. Acta **360**, 137008 (2020). DOI: 10.1016/j.electacta.2020.137008.
38. V. Khanna, P. Sharma, and P. Mahajan, eds. *Innovations and Applications of Hybrid Nanomaterials*. 2024, IGI Global: Hershey, PA, USA. 1.
39. R. Devi, V. Kumar, S. Kumar, M. Bulla, S. Sharma, and A. Sharma, Appl. Sci. **13**, 7907 (2023). DOI: 10.3390/app13137907.
40. S. Zhang, C. Lin, J. Ye, D. Zhao, Y. Chen, J.-M. Zhang, J. Tao, J. Li, Y. Lin, S. F. L. Mertens, O. V. Kolosov, and Z. Huang, Ceram. Int. **49**, 22160 (2023). DOI: 10.1016/j.ceramint.2023.04.043.
41. M. Ates and Y. Yuruk, Ionics **27**, 2659 (2021). DOI:10.1007/s11581-021-04007-y.
42. F. J. Hameed and I. M. Ibrahim, Iraqi J. Sci. **62**, 1503 (2021). DOI: 10.24996/ijs.2021.62.5.14.

تحضير المركب النانوي $PPy\text{-}MnO_2$ لاستخدامه في تطبيقات المكثفات الفائقة

فراس جاسم حميد[1] و عصام محمد ابراهيم[1]

[1]قسم الفيزياء، كلية العلوم، جامعة بغداد، بغداد، العراق

الخلاصة

لقد تم تحضير مركب البولي بايرول PPy باستعمال الاكسدة الكيميائية وتمت معالجتها بأوكسيد المنغنيز النانوي MnO_2 وتم تحضيرها وخلطها بنسب مختلفة وهي(10%، 30%، 50%). ولقد تم فحص المركب المتكون من PPyوMnO_2 بواسطة حيود الاشعة السينية لمعرفة الخصائص التركيبية وكذلك تم فحص المركب بواسطة التحليل الطيفي لمعرفة التركيب الجزيئي للمواد الأولية والمنتج النهائي للمركبات النانوية PPy و MnO_2 و PPy- MnO_2 ولقد بين في فحص FESEM ان سطح المادة يتكون من شبكة من الالياف النانوية. لقد تم تحضير المركب النانوي وذلك من خلال خلط مركب بولي بايرول PPy ذات الالياف النانوية مع مركب اوكسيد المنغنيز MnO_2 بنسب حجمية مختلفة حيث هذه النسب هي (10%، 30%، 50%) . وان اضافة اوكسيد المنغنيز الى البولي بايرول الى ادت الى زيادة الجسيمات النانوية الكروية على شبكة الالياف النانوية بشكل تدريجي حسب النسب السابقة. وقد ادت هذه الاضافة الى تغيير ملحوظ في التركيب البلوري للمركب النانوي. ولقد بين المركب النانوي انه يحمل صفات سعوية وبشكل كبير.حيث لوحظ ان اعلى سعة له هي 236 فاراد لكل غرام عندما كانت نسبة الاضافة هي 30% من اوكسيد المنغنيزفي حين ان السعة التي ظهر بها في المركب البولي بايرول النقي هي 125 فاراد لكل غرام .

الكلمات المفتاحية: بولي بايرول (PPy)، اوكسيد المنغنيز(MnO_2) ، الخواص التركيبية، المكثف الفائق، المتسعة.